Miniaturized Circularly-Polarized Patch Antenna Using an Artificial Metamaterial Substrate

Jamal Zaid* and Tayeb A. Denidni

Abstract—An artificially two-dimensional metamaterial (ATDM) substrate is proposed as an artificial metamaterial high-constitutive parameter substrate for miniaturizing of a circularly-polarized microstrip antenna. In a circularly-polarized antenna, the electric and magnetic field directions are changing, which requires a two-dimensional metamaterial unit cell. The presented ATDM substrate raises the permeability and permittivity of the underneath substrate for a circularly-polarized patch antenna, and it is constructed of periodically arranged split-ring resonator (SRR) circuits implemented in a low permittivity dielectric underneath substrate. The ATDM attains equal permittivity and permeability material ($\varepsilon_r \cong \mu_r$), which neutralizes the destructive effect of the increased permittivity on the bandwidth. In addition, the ATDM structure is implemented in printed circuit board technology. The area of the ATDM antenna at 2.45 GHz is approximately 75% smaller than a usual microstrip antenna. The proposed antenna bandwidth is enhanced compared to the antennas with high-permittivity substrates. The proposed ATDM substrate antenna is fabricated and measured, and comparisons show good agreements between simulated and measured results.

1. INTRODUCTION

Microstrip patch antennas can be printed directly onto a circuit board, and have a low profile and are easily fabricated [1]. One major drawback in a patch antenna is its large size. Several different techniques have been proposed in literature for miniaturizing the antennas [2–16]. In [2–5], miniaturization is achieved by using geometrical modification. In these methods, the electrical length of the current path is increased, which leads to miniaturization of the antenna. However, all these approaches can only work for linear polarization.

In [6], a substrate with a high amount of permittivity has been proposed which is a popular method. In this technique, the electrical energy density in the substrate increases due to the increasing permittivity. As a result, the impedance on the radiating edge raises, which becomes difficult to feed the antenna by a quarter-wavelength impedance transformer. Furthermore, surface waves will excite by the increased permittivity, thereby decreasing the radiation efficiency. Moreover, enhancing the electrical energy density in the underneath substrate enhance the quality factor (Q), which decreases the bandwidth.

Another technique, based on magneto-dielectric substrates, has been used for miniaturizing microstrip-patch antennas. Researchers in [7–9] have created a magneto-dielectric substrate using an array of parallel split-ring resonators (SRRs). Employing these array leads to a better reflection coefficient bandwidth as compared to high-permittivity substrates [6]. However, these designs are huge, and their prototyping leads to a bulky structure compared to that of antenna with conventional substrates. Moreover, the fabrication of these types of substrates is complicated because of the several

parallel layers that should be placed under the patch. A planar magneto-dielectric substrate has been proposed in [10–15]. Although these types of substrates are planar, the antenna efficiency is less than the one with un-planar magneto-dielectric substrate [7–9]. Recently, a new fabrication technology has emerged for the design of polymer-based magneto-dielectric composite substrates for antennas, such as nickel and ferrite [16, 17]. Such composite substrates have a better performance compared to artificially magneto-dielectric substrates due to its homogeneous structure. It enhances the antenna bandwidth and reduces the antenna size while maintaining good efficiency and gain.

The characteristic impedance of a magneto-dielectric substrate ($\eta = \eta_o \sqrt{\varepsilon_r/\mu_r}$) will be nearly equal to the characteristic impedance of the free space (η_o) if the value of relative permittivity and relative permeability are equal ($\varepsilon_r/\mu_r \cong 1$). This allows to achieve a large impedance bandwidth because of the improved impedance matching conditions among the two radiating edges in the patch antenna and in free space. In these substrates [7–11], the magnetic-field vectors have to be perpendicular to the SRR loops in order to achieve the desired functioning. However, in a circularly-polarized antenna, the magnetic-field vectors rotate with time at a steady rate; thus these types of substrate cannot be employed in circularly-polarized antenna, which represents the biggest drawback of these substrates. In addition, these substrate structures are difficult to implement.

To overcome these problems, a novel artificially two-dimensional metamaterial (ATDM) substrate is proposed in this paper. This two-dimensional metamaterial substrate is developed for the design of a circularly-polarized antenna. The structure can be realized in planar technology. This substrate increases the magnetic permeability, which counterbalances for the bandwidth degradation that occurs due to the raised permittivity. We designed a miniaturized circularly-polarized microstrip patch antenna with the proposed ATDM substrate; that antenna was then fabricated and its performance was measured. Comparisons show good agreements between simulated and measured results.

2. CIRCULARLY-POLARIZED MICROSTRIP ANTENNA AND ARTIFICIALLY TWO-DIMENSIONAL METAMATERIAL SUBSTRATE

The most commonly employed microstrip antenna is a rectangular patch that looks like a microstrip transmission line. It is approximately one-half wavelength long [1]. The antenna frequency can be calculated as

$$f = \frac{c}{2(L+h)\sqrt{\varepsilon_e \mu_e}} \tag{1}$$

$$\varepsilon_e = \frac{\varepsilon_r+1}{2} + \frac{\varepsilon_r-1}{2}\left(1 + \frac{12h}{W}\right) \tag{2}$$

where L and W are the length and width of the rectangular patch, respectively; ε_r is the relative permittivity of the substrate; μ_r is the relative permeability of the substrate; ε_e and μ_e are the effective electric permittivity and effective permeability of a dielectric substrate, respectively; and h is the thickness of the substrate. If two orthogonal patch modes of a single-point feed patch antenna are simultaneously excited with equal amplitude and $\pm 90°$ out of phase, it can radiate circular polarization. Various shapes for single-point feed microstrip antennas, capable of circular polarization operation, can be found in the literature. In [18], a truncated-corner method has been proposed to obtain circularly-polarized antenna. By using this method, the antenna resonance frequency is approximately like that of a conventional rectangular patch antenna. As can be seen from Eq. (1), by increasing the ε_r and μ_r of the host substrate, the resonance frequency will be decreased for a fixed dimension. This means that the antenna can be miniaturized by raising the constitutive parameters (ε_r, μ_r) of the substrate.

In this paper, we design an ATDM substrate that can work with circularly-polarized patch antennas. The proposed ATDM substrate is constructed of an array of unit cells in the x and y-axes, as depicted in Fig. 1. It contains SRR loops along the x and y-axes, where each functions with linear-polarization excitation in the x and y-axes, respectively. A circularly-polarized electromagnetic wave is composed of two linearly-polarized modes with $\pm 90°$ out of phase and equal amplitude. Therefore, in the case of a circularly-polarized antenna, two orthogonal modes can be assumed in the x and y-axes, where the x-axis mode excites the x-axis unit cells, and the y-axis mode excites the y-axis unit cells. The proposed substrate thus operates as an artificially two-dimensional metamaterial (ATDM) substrate.
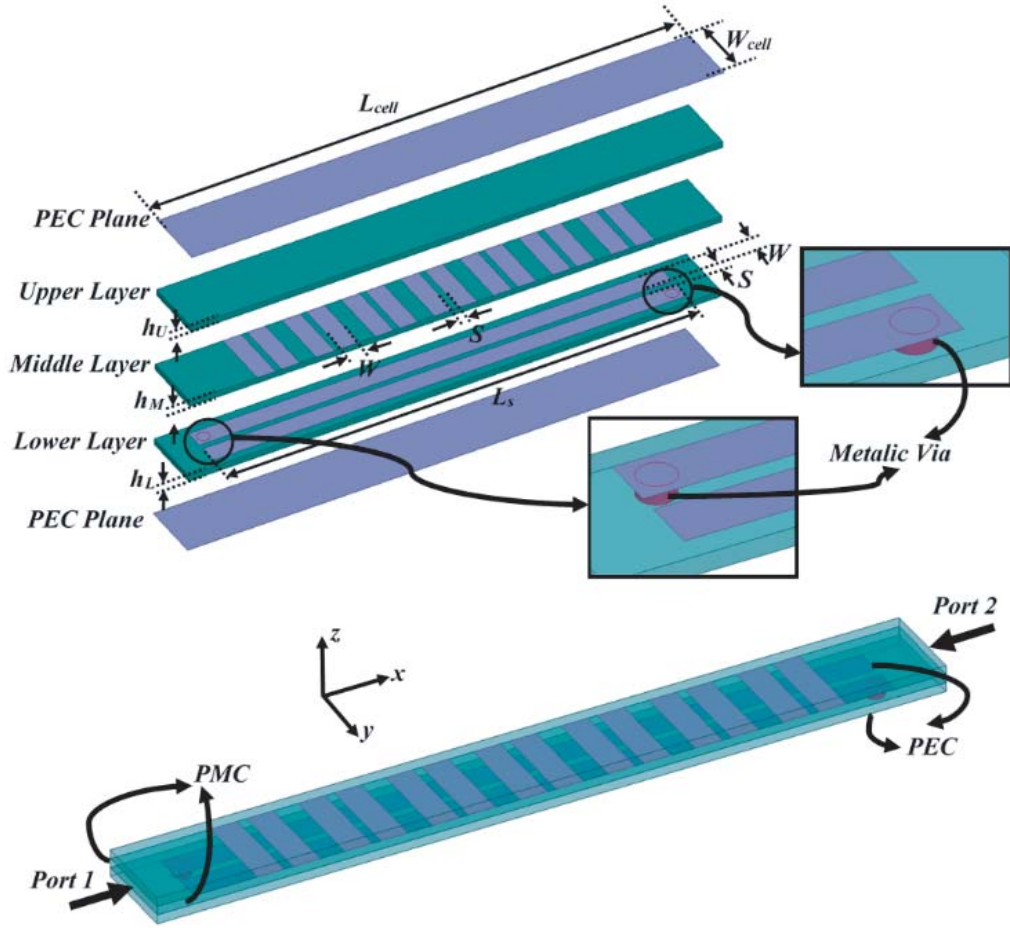
Figure 1. Perspective view of the proposed ATDM unit cell. The dimensions are $W = 0.35$, $S = 0.1$, $h_L = h_M = h_U = 0.203$, $L_s = 15.4$, $L_{cell} = 17.5$, $W_{cell} = 2.5$, all in millimeters.

The equivalent circuit of the ATDM unit cell is illustrated in Fig. 2. If we consider the unit cell as an electric circuit, then by using the telegrapher's equations for the equivalent model depicted in Fig. 2, the equivalent inductance can be driven, given by

$$L_{eq} = \frac{V_1 - V_2}{j\omega I_1} = L_l \left(1 - k^2 \frac{1}{1 - \frac{\omega_p^2}{\omega^2}} \right) \tag{3}$$

where $\omega_p = 1/\sqrt{L_p C_p}$ is the resonant frequency of the SRR-like loop, also known as the plasma frequency, and $k = M/\sqrt{L_l L_p}$ is the coupling coefficient. The equivalent inductance given in Eq. (3) is higher than the inductance of the base line at frequencies lower than the resonant frequency; the equivalent inductance approaches infinity as the frequency approaches the resonant frequency.

The parameters L_l, L_p, and M determine the electrical performance and can be easily estimated for the unit cell model depicted in Fig. 2. The magnetic field can be considered as $\hat{y}H_0$, and hence, the magnetic flux can be calculated as $\Phi = \mu_0 H_0 L_{cell}(h_L + h_M + h_U)$, and based on the boundary condition, the current on the line is $I = H_0 W_{cell}$. Therefore, the inductance of the line will be $L_l = \Phi/I = \mu_0 L_{cell}(h_L + h_M + h_U)/W_{cell}$. The self-inductance of the loop can be approximately estimated as

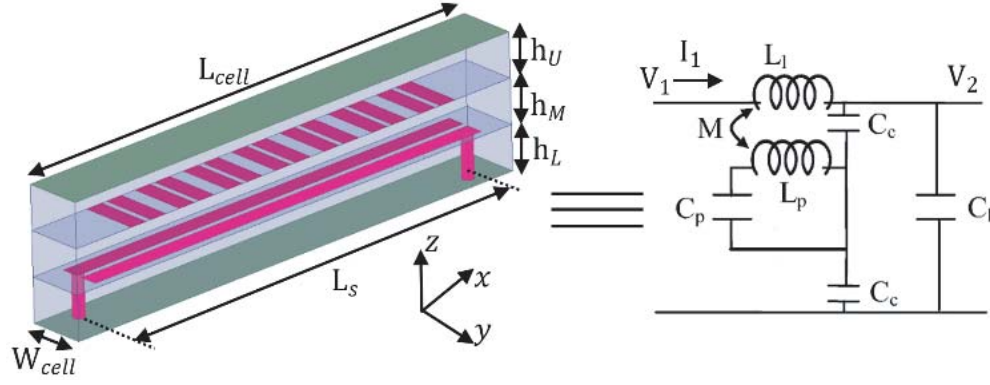$$L_p = \frac{\mu_0 A_p}{W_{cell}} = \frac{\mu_0 L_s h_L}{W_{cell}} \tag{4}$$

Figure 2. Equivalent circuit of the ATDM unit cell.

where A_p is the area of the SRR-like loop. The mutual inductance can also be calculated as

$$M = \frac{\mu_0 A_p}{W_{cell}} \tag{5}$$

and the coupling coefficient can be given as

$$k^2 = \frac{M^2}{L_l L_p} = \frac{L_s h_L}{L_{cell}(h_L + h_M + h_U)} < 1$$

Using a reverse process the equivalent permeability ATDM substrate can be obtained from Eq. (2) as

$$\mu_{eff} = \mu_0 \left(1 - k^2 \frac{1}{1 - \frac{\omega_p^2}{\omega^2}} \right) \tag{6}$$

A glance at the equivalent circuit in Fig. 2 shows that the equivalent capacitance will be driven as

$$C_{eq} = C_l + \frac{C_c}{2}$$

By using the conformal mapping technique, the capacitance between a thin strip and a perfect conductor (C_c) can be calculated as [19]

$$C_c = 2\frac{\varepsilon K\left(\sqrt{1-g^2}\right)}{K(g)} \tag{7}$$

$$g = \frac{h}{h+W} \tag{8}$$

where K is the elliptic integral defined by

$$K(g) = \int_0^{\frac{\pi}{2}} \frac{d\emptyset}{\sqrt{1 - g^2 sin^2(\emptyset)}} \tag{9}$$

In view of the above discussion, the effective permittivity of the medium can be then calculated from

$$\varepsilon_{eff} = \varepsilon \left[1 + \frac{(h_L + h_M + h_U)L_s}{L_{cell}W_{cell}} \frac{K\left(\sqrt{1-g^2}\right)}{K(g)} \right] \tag{10}$$

The constitutive parametric quantities of the substrate are extracted using the technique reported by Shi et al. [20] under the given boundary conditions depicted in Fig. 1. The xz-plane walls are perfect magnetic conductors (PMCs), and the xy-plane walls are perfect electric conductors (PECs).

The effective constitutive parameters are extracted and can be considered as the effective constitutive parametric quantities of the whole ATDM substrate (Fig. 3). The frequency response of the ATDM unit cell depends on the unit cell dimensions. The SRR-like length (L_s) is the most important parameter that influences the resonance frequency of the ATDM unit cell; the resonance frequency of the SRR-like resonator decreases by increasing its length L_s. An array of 7×7 unit cells will then make the whole ATDM substrate. The patch is printed on the upper substrate, and the truncated-corner technique is employed to obtain a circularly-polarized antenna (Fig. 4). In this case, Rogers RO4003 substrate is employed as the host substrate. The antenna resonance frequency is considered to be at 2.45 GHz. Thus the resonance frequency of the designed unit cell must be set at a slightly higher frequency than
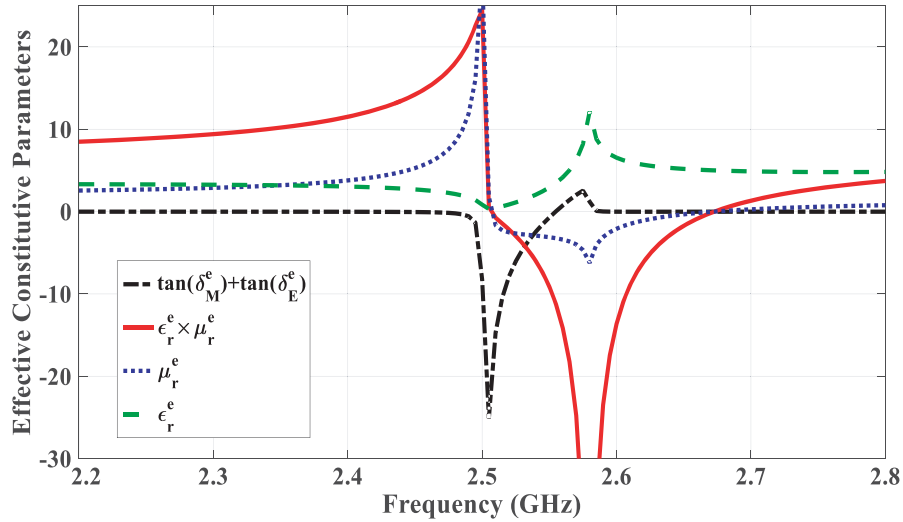

Figure 3. Effective constitutive parametric quantities of the ATDM substrate, and the electric and magnetic losses. The product of the dielectric permittivity and magnetic permeability constants is also shown.
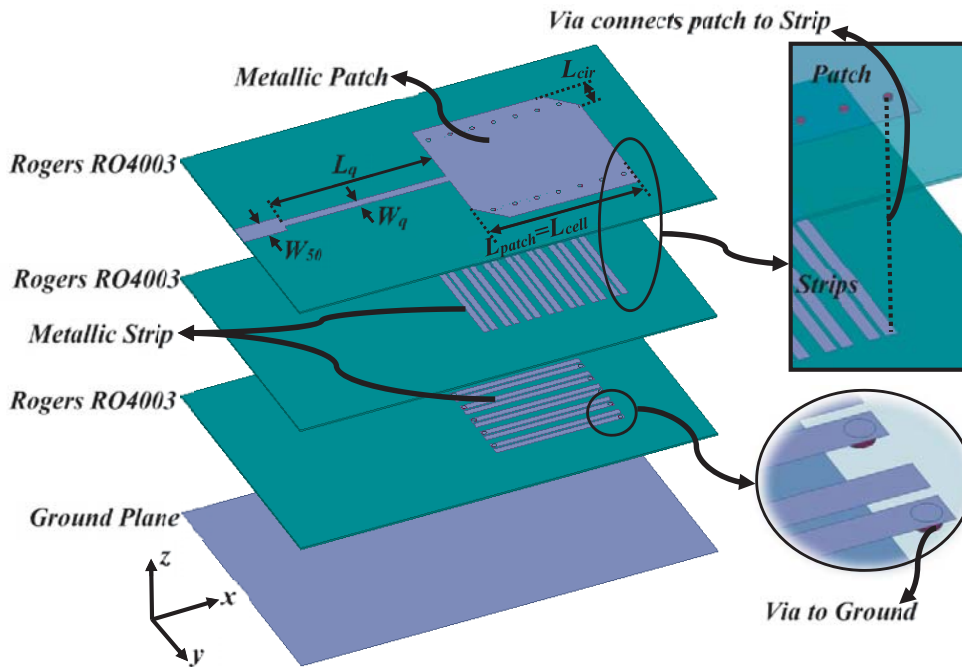

Figure 4. Microstrip patch antenna with the proposed ATDM substrate.

the antenna resonance frequency, because, as can be seen from Fig. 3, the electrical and magnetic losses are high around the resonance frequency of the unit cell. On the other hand, by moving to the lower frequency in Fig. 3, the product of the ATDM permittivity and the permeability constants decreases.

3. RESULTS AND DISCUSSIONS

The ATDM antenna is compared to other equivalent substrates, defined in Table 1. In case-2 and case-3, the patch size and substrate thickness are the same as in the proposed ATDM substrate (case-1). The dimensions in these cases are L_{patch}= 18, W_q= 0.3, L_q= 19, L_{cir}= 3, W_{50}= 1.3, L_{50}= 7, all in millimetres. In case-4, the thickness of the substrate is the same as case-1, but the patch dimensions are set to the antenna resonance frequency at 2.45 GHz. In this case, the dimensions are L_{patch}= 34, W_q= 0.4, L_q= 19, L_{cir}= 4, W_{50}= 1.3, L_{50}= 7, all in millimetres. Each of the four cases was simulated using Ansys HFSS software. The simulation results are summarized in Table 2, and the S-parameters are shown in Fig. 5. By comparing the results of case-1 and case-2 in Table 2, it can be concluded that the calculated constitutive parametric quantities of the ATDM unit cell well modelled the substrate in case-2 at the frequency of 2.45 GHz. Between case-1 and case-2, there is only a 45 MHz frequency shift. For case-2, the magnetic and electric losses are set as the magnetic and electric losses of case-1 at the 2.45 GHz frequency. Nevertheless, the radiation efficiency is improved in case-2, because the substrate is homogeneous. Case-3 is a high-permittivity dielectric substrate antenna with permeability equal to

Table 1. Defined cases of the substrate for evaluating the potentials and limitation of the ATDM substrate.

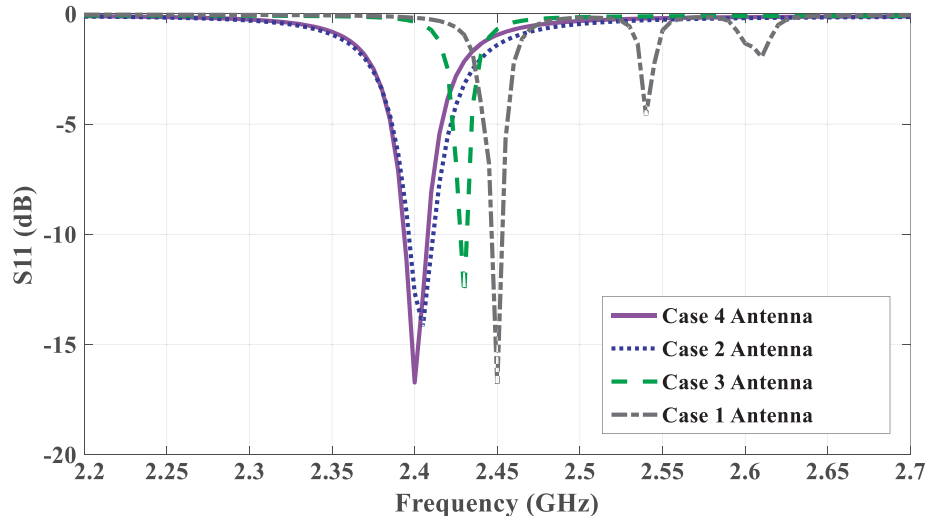| Case	Substrate
1	Proposed ATDM Substrate Antenna.
2	An equivalent substrate with $\varepsilon_r = \varepsilon_r^e(f_c = 2.45\,\text{GHz})$, $\mu_r = \mu_r^e(f_c = 2.45\,\text{GHz})$, $\tan\delta_e = \tan\delta_e^e(f_c = 2.45\,\text{GHz})$, $\tan\delta_m = \tan\delta_m^e(f_c = 2.45\,\text{GHz})$.
3	An equivalent substrate with $\varepsilon_r = \varepsilon_r^e(f_c = 2.45\,\text{GHz}) \times \mu_r^e(f_c = 2.45\,\text{GHz})$, $\mu_r = 1$, $\tan\delta_e = \tan\delta_e^e(f_c = 2.45\ GHz) + \tan\delta_m^e(f_c = 2.45\,\text{GHz})$.
4	Conventional Antenna with Rogers RO4003 substrate.


Figure 5. Input return losses of the defined cases in Table 1.

Table 2. Simulation results of the cases defined in Table 1.

Case	Frequency	BW $-10\,\mathrm{dB}$	BW %	Gain	$\eta_r = G/D$
1	2.45 GHz	12 MHz	0.48	2.8 dBic	55%
2	2.4 GHz	20 MHz	0.83	4.6 dBic	65%
3	2.427 GHz	8 MHz	0.32	1.6 dBic	30%
4	2.45 GHz	20 MHz	0.81	6.25 dBic	80%

1, and a permittivity equal to the product of ε_r and μ_r of the ATDM substrate. The patch size is the same as in the ATDM substrate of case-1. As can be seen from Table 2, the bandwidth of the ATDM substrate antenna is better than the bandwidth in case-3. In case-4, Rogers RO4003 is used as the substrate. The size of the patch is $34 \times 34\,\mathrm{mm}^2$, compared to the ATDM substrate's antenna, which is $18 \times 18\,\mathrm{mm}^2$. In case-1, the size of the antenna is decreased by 75%, while the bandwidth is not reduced compared to case-3.

Figure 6 shows photos of the fabricated ATDM substrate antenna. The simulated and measured input return losses of the ATDM substrate antenna are depicted in Fig. 7. Those input return losses in Fig. 7 reveal a 13 MHz frequency shift between simulated and measured results, attributed to fabrication accuracy and tolerance the permittivity tolerance of ± 0.05. Antenna efficiency is a handy parameter for evaluating the antenna performance with omni-directional radiation pattern because it does not take into account radiation direction. In other words, the antenna gain is a preferable parameter for evaluating the antenna performance, if the antenna is designed to radiate as a directive antenna. A quad-ridge measurement antenna is used to separate the vertical and horizontal components of received energy. Notice that the vertical and horizontal components of a CP waves are 90° out of phase. This is measured as a 90° phase shift in our laboratory. Whether there is an advance or delay by 90° between the vertical and horizontal components, tells us if the wave is RHCP or LHCP. Fig. 8 shows a practical antenna measurement setup. The measured and simulated axial ratios of the ATDM substrate antenna versus frequency in broadside (z-axis) are shown in Fig. 9(c). The measured right-hand circular-polarization (RHCP) axial ratio bandwidth is 13 MHz, which covers the S_{11} bandwidth, compared to case-3's (high-permittivity substrate) simulated RHCP axial ratio, which is reduced to 4 MHz. The RHCP patch's surface current variations for different phases at the centre frequency of 2.45 GHz are
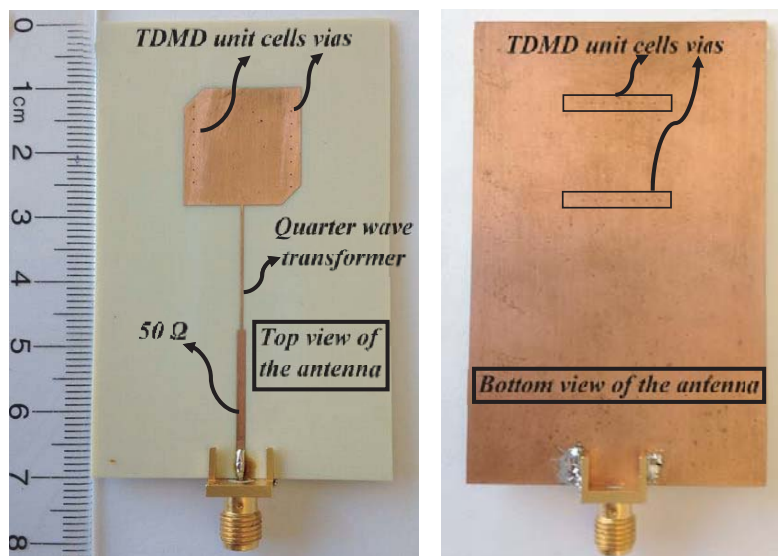
Figure 6. Top and bottom views of the fabricated ATDM substrate antenna.
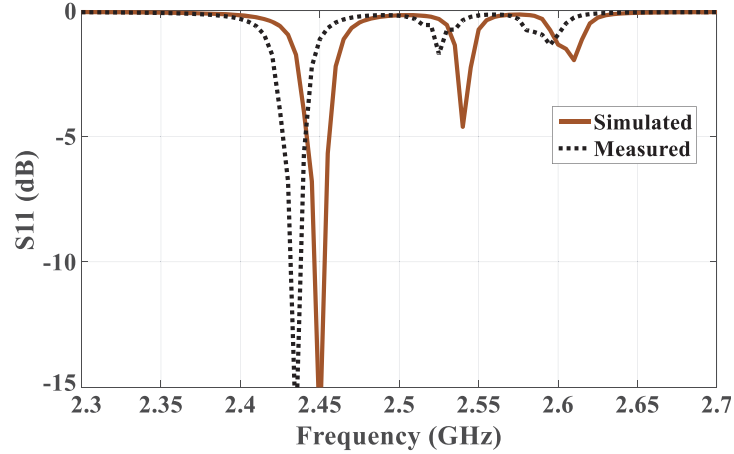
Figure 7. Measured and simulated input return losses of the proposed ATDM substrate antenna.
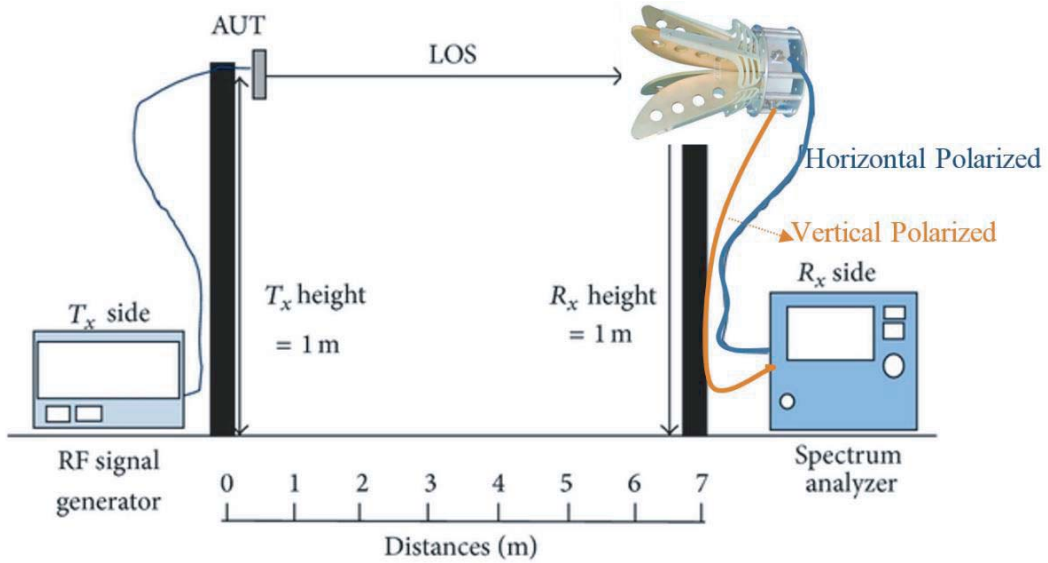

Figure 8. The practical antenna measurement setup.

shown in Fig. 9(a), and the RHCP SRR-like loop current variations for different phases at the center frequency of 2.45 GHz are shown in Fig. 9(b). Fig. 9(b) is plotted in order to better understand how the artificially two-dimensional metamaterial substrate is achieved by an array of one-dimensional unit cells. The measured and simulated radiation pattern of the proposed ATDM substrate antenna is shown in Fig. 10. Case-4 (conventional antenna without miniaturization) obviously has the highest gain (Table 2) among all four cases. However, its size is quite larger. This is because the distance between the two radiating edges on the patch is reduced by miniaturizing the patch antenna; it is not connected with antenna efficiency. The decrease in gain is due to the decreasing the distance between two radiating-edges similar to antenna arrays. By decreasing the inter-element spacing in antenna arrays, the gain will reduce a little. Nevertheless, the gain differences among the first three cases are because of the different antenna efficiencies. Case-3 (high-permittivity substrate) has the lowest gain because of the fact that it has the worst mismatch condition that can occur between the two radiating edges and free space $(\eta = \eta_o \sqrt{\varepsilon_r/\mu_r} \neq \eta_o)$. Case-2 is the optimal matching condition $(\varepsilon_r/\mu_r = 1)$, and as a result, it obtains the highest possible gain. In case-1 (the proposed ATDM substrate antenna), although the permittivity and permeability are equal $(\varepsilon_r \cong \mu_r)$, the gain is slightly less than that of case-2 because of the metallic losses in the SRR-like loops.
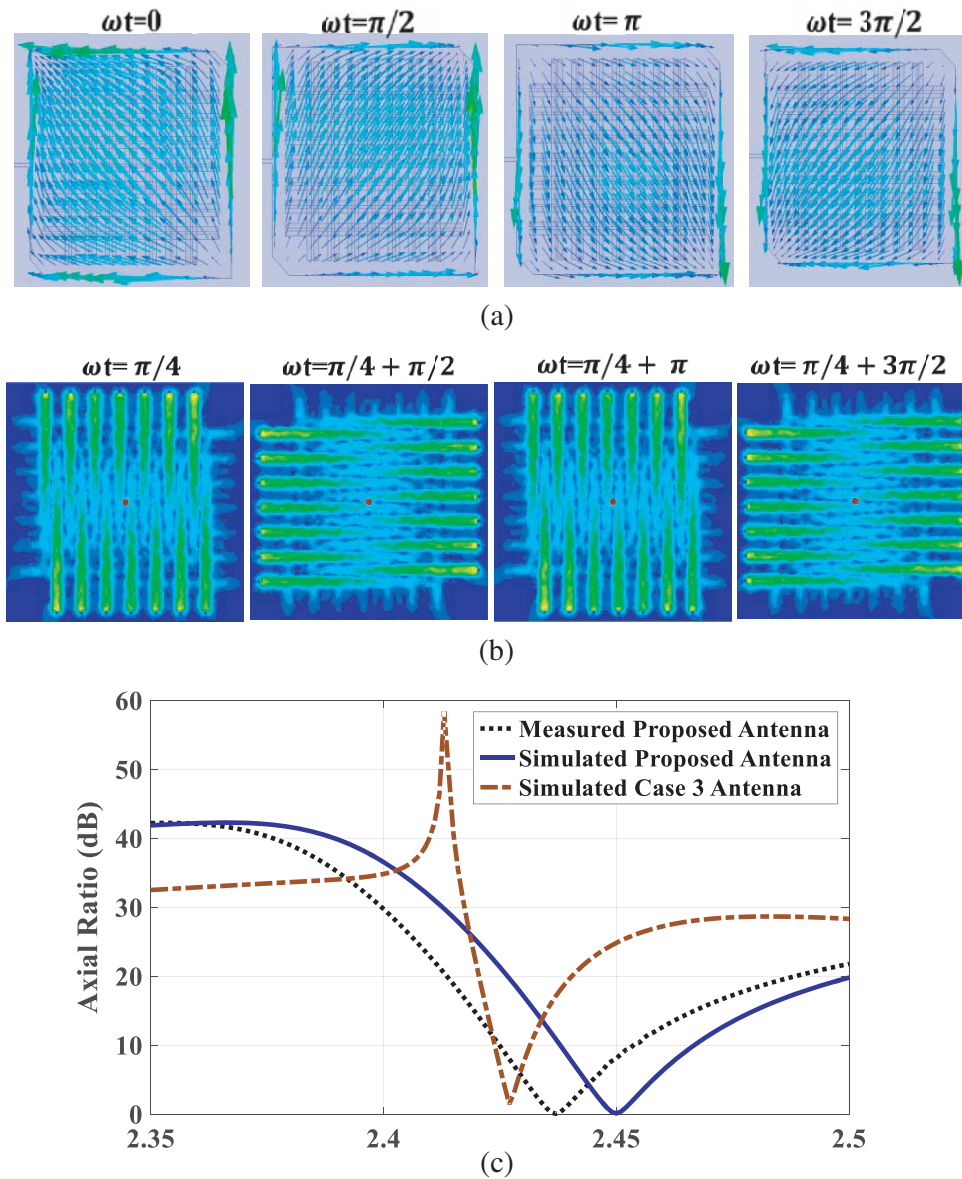
Figure 9. Axial ratio and current variations of the proposed ATDM substrate antenna. (a) RHCP patch surface current variations at different phases at 2.45 GHz. (b) RHCP SRR-like lope current variations at different phases at 2.45 GHz. (c) Measured and simulated axial ratio of the proposed ATDM substrate antenna versus frequency in broadside (z-axis). Simulated axial ratio of the case-3 antenna (defined in Table 1) is also shown for comparison.

Table 3 shows the resonance frequency, miniaturization ratio, gain, frequency bandwidth, and radiation efficiency of the proposed antenna compared to other techniques reported in the literature. These techniques are only applicable for linear polarized antennas in general. The novelty of this work is that a two-dimensional metamaterial substrate is designed for miniaturization of circularly polarized antennas. In References [7–11] and [13], the magnetic field vectors have to be perpendicular to the SRR loops in order to achieve the desired operation. However, in circularly-polarized antennas, the magnetic field vectors rotate with time at a steady rate, and thus these types of substrate cannot be employed in circularly-polarized antennas, which represents these substrates' major weakness.

Table 3. Comparison of the proposed antenna with those from selected references.

	F_0 (GHz)	BW (%)	Gain	η (%)	Normalized Radiating Patch Dimension (λ_0^3)	Total Antenna Dimension (mm³)	MR[a] %
This Work	2.45	0.48	2.8 dBic	55	$0.24 \times 0.33 \times 009$	$43 \times 70 \times 0.609$	75
[7]	2.48	0.08	-2 dBi	30	$0.33 \times 0.372 \times 0.066$	$80 \times 80 \times 8$	37
[8]	1.74	0.6	-	35	$0.23 \times 0.22 \times 0.017$	$39.6 \times 38.4 \times 3$	69
[9]	2	5	7 dBi	87	$0.26 \times 0.232 \times 0.06$	$100 \times 100 \times 10$	15
[10]	2.34	0.5	1.34 dBi	48	$0.25 \times 0.344 \times 009$	$50 \times 70 \times 1.219$	74
[11]	2.55	1.6	5.6 dBi	-	$0.68 \times 0.68 \times 0.051$	$80 \times 80 \times 1.6$	34
[13]	2.48	0.48	3.2 dBi	45	$0.392 \times 0.48 \times 008$	$45 \times 75 \times 1.016$	67
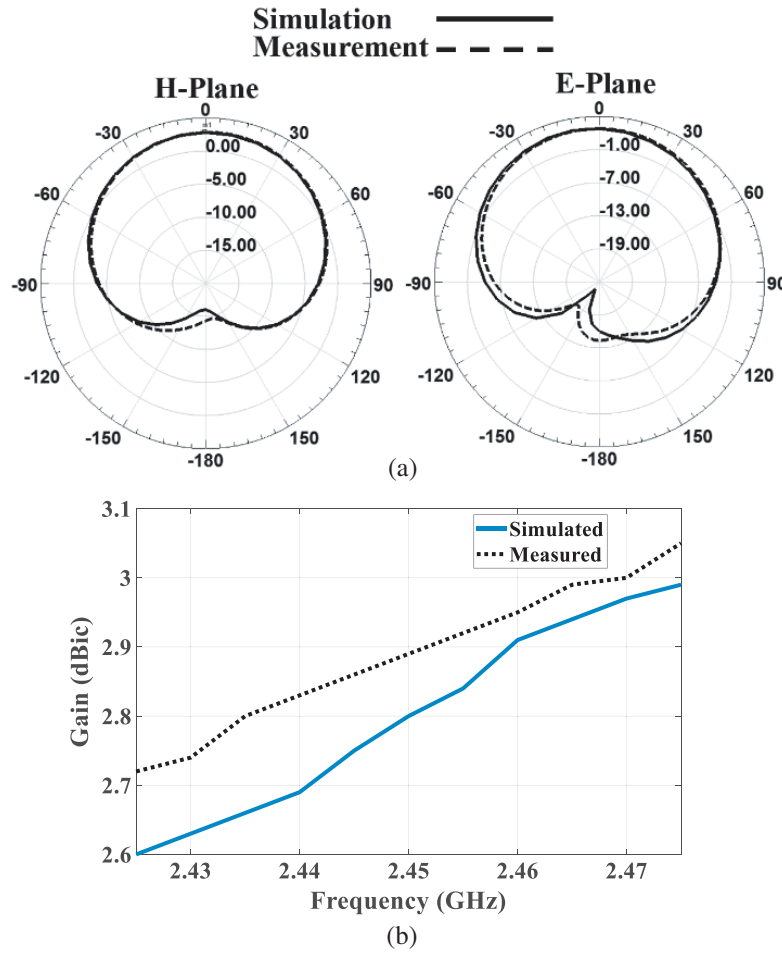
Figure 10. Measured and simulated radiation pattern of the proposed ATDM substrate antenna. (a) Radiation pattern at 2.45 GHz. (b) Maximum gain versus frequency.

4. CONCLUSION

In this paper, we have presented a design for an artificially two-dimensional metamaterial substrate that can work with circularly-polarized antennas. The proposed structure has been used for miniaturizing a circularly-polarized patch antenna whereas the other artificial magneto-dielectric unit cells cannot be employed in circularly-polarized antennas. Using the proposed ATDM substrate, a circularly-polarized patch antenna has been designed at 2.45 GHz. The antenna size has been reduced by 75%. The constitutive parametric quantities of the ATDM substrate have been calculated, and the ATDM substrate ability to obtain better bandwidth characteristics than high-permittivity substrates has been investigated. Finally, the prototype of the antenna has been made and measured, and comparisons have shown good agreements between simulated and measured results.The proposed antenna is suitable for several applications such as, Radio Frequency Identification (RFID), Global Position System (GPS) and Wi-Fi.

REFERENCES

1. Balanis, C. A., *Antenna Theory: Analysis and Design*, 2nd Edition, Wiley, New York, 1997.
2. Esfahlani, S. H. S., A. Tavakoli, and P. Dehkhoda, "A compact single-layer dual-band microstrip antenna for satellite applications," *IEEE Antennas Wireless Propag. Lett.*, Vol. 10, 931–934, 2011.
3. Chakraborty, U., A. Kundu, S. K. Chowdhury, and A. K. Bhattacharjee, "Compact dual-band microstrip antenna for IEEE 802.11a WLAN application," *IEEE Antennas Wireless Propag. Lett.*, Vol. 13, 407–410, 2014.
4. Reddy, B. R. S. and D. Vakula, "Compact Zigzag-shaped-slit microstrip antenna with circular defected ground structure for wireless applications," *IEEE Antennas Wireless Propag. Lett.*, Vol. 14, 678–681, 2015.
5. Wong, K. and H. Tung, "An inverted U-shaped patch antenna for compact operation," *IEEE Trans. Antennas Propag.*, Vol. 51, No. 7, 1647–1648, 2003.
6. Colburn, J. S. and Y. Rahmat-Samii, "Patch antennas on externally perforated high dielectric constant substrates," *IEEE Trans. Antennas Propag.*, Vol. 47, No. 12, 1785–1794, 1999.
7. Mookiah, P. and K. R. Dandekar, "Metamaterial-substrate antenna array for MIMO communication system," *IEEE Trans. Antennas Propag.*, Vol. 57, No. 10, 3283–3292, 2009.
8. Mosallaei, H. and K. Sarabandi, "Design and modeling of patch antenna printed on magneto-dielectric embedded-circuit metasubstrate," *IEEE Trans. Antennas Propag.*, Vol. 55, No. 1, 45–52, 2007.
9. Pinsakul, A., S. Chaimool, and P. Akkaraekthalin, "Miniaturized microstrip patch antenna printed on magneto-dielectic metasubstrate," *2012 9th International Conference on Electrical Engineering/Electronics, Computer, Telecommunications and Information Technology (ECTI-CON)*, 1–4, Phetchaburi, 2012.
10. Kumar, S. and D. K. Vishwakarma, "Miniaturisation of microstrip patch antenna using an artificial planar magneto-dielectric meta-substrate," *IET Microw. Antennas Propag.*, Vol. 10, No. 11, 1235–1241, 2016.
11. Kim, D., "Planar magneto-dielectric metasubstrate for miniaturization of a microstrip patch antenna," *Microw. Opt. Technol. Lett.*, Vol. 54, No. 12, 2871–2874, 2012.
12. Farahani, M., J. Zaid, T. A. Denidni, and M. Nedil, "Miniaturized two dimensional circular polarized magneto-dielectric substrate antenna," *2016 IEEE International Symposium on Antennas and Propagation (APSURSI)*, 1103–1104, Fajardo, 2016.
13. Farzami, F., K. Forooraghi, and M. Norooziarab, "Miniaturization of a microstrip antenna using a compact and thin magneto-dielectric substrate," *IEEE Antennas Wireless Propag. Lett.*, Vol. 10, 1540–1542, 2011.
14. Farahani, M., M. Akbari, M. Nedil, A. R. Sebak, and T. A. Denidni, "Miniaturised circularly-polarised antenna with high-constitutive parameter substrate," *Electronics Letters*, Vol. 53, No. 20, 1343–1344, September 28, 2017.

15. Zaid, J., M. Farahani, and T. A. Denidni, "Magneto-dielectric substrate-based microstrip antenna for RFID applications," *IET Microwaves, Antennas & Propagation*, Vol. 11, No. 10, 1389–1392, August 16, 2017.

16. Borah, K. and N. S. Bhattacharyya, "Magneto-dielectric material with nano ferrite inclusion for microstrip antennas: Dielectric characterization," *IEEE Trans. on Dielectrics and Electrical Insulation*, Vol. 17, No. 6, 1676–1681, 2010.

17. Algadami, A. S. M., M. F. Jamlos, P. J. Soh, and M. R. Kamarudin, "Polymer (PDMS-Fe$_3$O$_4$) magneto-dielectric substrate for MIMO antenna array," *Appl. Phys. A*, Vol. 122, No. 9, 2016.

18. Sharma, P. and K. Gupta, "Analysis and optimized design of single feed circularly polarized microstrip antennas," *IEEE Trans. Antennas Propag.*, Vol. 31, No. 6, 949–955, 1983.

19. Smythe, W. R., *Static and Dynamic Electricity*, McGraw Hill, New York, 1968.

20. Shi, Y., Z. Y. Li, K. Li, L. Li, and C. H. Liang, "A retrieval method of effective electromagnetic parameters for inhomogeneous metamaterials," *IEEE Trans. Micow. Theory Tech.*, Vol. 65, No. 4, 1160–1178, 2017.